

Damage mechanism and stress response of reinforced concrete slab under blast loading

K. Senthil^{*}, A. Singhal^a and B. Shailja^b

Department of Civil Engineering, Dr. B R Ambedkar National Institute of Technology Jalandhar, Jalandhar, Punjab 144011, India

(Received February 3, 2019, Revised May 15, 2019, Accepted June 4, 2019)

Abstract. The numerical investigations have been carried out on reinforced concrete slab against blast loading to demonstrate the accuracy and effectiveness of the finite element based numerical models using commercial package ABAQUS. The response of reinforced concrete slab have been studied against the influence of weight of TNT, standoff distance, boundary conditions, influence of air blast and surface blast. The results thus obtained from simulations were compared with the experiments available in literature. The inelastic behavior of concrete and steel reinforcement bar has been incorporated through concrete damage plasticity model and Johnson-cook models available in ABAQUS were presented. The predicted results through numerical simulations of the present study were found in close agreement with the experimental results. The damage mechanism and stress response of target were assessed based on the intensity of deformations, impulse velocity, von-Mises stresses and damage index in concrete. The results indicate that the standoff distance has great influence on the survivability of RC slab against blast loading. It is concluded that the velocity of impulse wave was found to be decreased from 17 to 11 m/s when the mass of TNT is reduced from 12 to 6 kg. It is observed that the maximum stress in the concrete was found to be in the range of 15 to 20 N/mm² and is almost constant for given charge weight. The slab with two short edge discontinuous end condition was found better and it may be utilised in designing important structures. Also it is observed that the deflection in slab by air blast was found decreased by 60% as compared to surface blast.

Keywords: reinforced concrete slab; damages; blast loading; mass of TNT; finite element analysis; deformation

1. Introduction

In the past few decades, damage to a structure due to explosion has increased as a result of increase in number and intensity of terrorist activities, manmade accident, and natural explosion during earthquake, climatic changes etc. In order to design structures which are able to withstand, it is necessary to first quantify the effects of such explosions. Typically, it is calculated from various sources such as professional guides, experimental tests and analytical tools. Nowadays, blast resistant design is becoming an important part of the design since the vulnerabilities due to

^{*}Corresponding author, Assistant Professor, E-mail: urssenthil85@yahoo.co.in, kasilingams@nitj.ac.in

^aPost Graduate Student, E-mail: eng.akhilsinghal92@gmail.com

^bAssistant Professor, E-mail: shailja.bawa@gmail.com

widespread terrorist activities. Keeping this in mind, research communities all over the world are seeking solutions for potential blasts, protecting building occupants and the structures. Ettouney *et al.* (1996) presented design of commercial building subjected to blast loading. It is observed that the design modifications and recommendations that improve ductility and structural response during occurrence of blast load. Watson *et al.* (2005) carried out experiments and measured the damages caused to reinforced concrete T beams and slabs by contact and close proximity explosive charges using different areas of contact and angles of inclination for the explosives. Experiments of blast on the prototype and model specimens were conducted and found in agreement between the prototype and model response. Osteras *et al.* (2006) discussed qualitative assessment of blast damage and collapse pattern of murrrah Building bombing in 1995. The destruction was mainly due to combination of direct blast effects that destroyed one column and large portions of the second, third and perhaps portions of the fourth floor slab. It is concluded that a complete three dimensional space frame that interconnects all load path provides stability. Ngo *et al.*, (2007) and Ngo and Mendis (2009) presents a comprehensive overview of the effects of explosion on structures. An explanation of the nature of explosions and the mechanism of blast waves in free air is given. Authors were introduced different methods to estimate blast loads and structural response. King *et al.* (2009) discussed typical building retrofit strategies for load bearing and non-load bearing structural members through strengthening, shielding, or controlling hazardous debris. Shi *et al.* (2009) also conducted numerical investigations to investigate the bond-slip effect on numerical analysis of blast-induced responses of a RC column. Wu *et al.* (2009) presented study on blast resistance of normal reinforced concrete (NRC), ultra-high performance fibre (UHPFC) and FRP-retrofitted concrete slab (RUHPFC). The results indicates that the plain UHPFC slab had a similar blast resistance to the NRC slab and that the RUHPFC slab was superior to both.

Wakchaure and Borole (2013) compared between long side and short side column and percentage of stress of reinforced concrete column for long and short side is presented an analysis is carried out using ANSYS. It was conclude that the critical impulse for the long column case found to be significantly higher. Samir (2014) performed numerical simulations on reinforced concrete columns subjected to various blast loads using the finite element software ABAQUAS. The effects of transverse and longitudinal reinforcement ratios, charge weight and column aspect ratio were the parameters considered. It was concluded that the residual displacement becomes more significant after a certain charge weight. Yi *et al.* (2014) presented new approach (Hybrid blast load method instead of pressure load or detonation simulation method) for the applications of blast loads on bridge components. Hybrid blast load method uses realistic loads and able to simulate both reflection and diffraction of blast loads using LS DYNA. It is concluded that the proposed model is advantageous over pressure load model as it predicts more conservative results. Burrel *et al.* (2015) present study on response of steel fiber-reinforced concrete (SFRC) column subjected to blast loading. It is concluded that SFRC improves the blast performance of columns in terms of maximum and residual displacements as well as damage tolerance and elimination of secondary blast fragments. Liu *et al.* (2015) presented simplified blast load effects on the column and bent beam of highway bridges using finite element model. Study shows that the above model may reproduce many of the damage mechanism of typical highway bridge. It is observed that the provision of transverse reinforcement improved the blast resistance of highway bridges. Wijesundara and Clubley (2016) also investigates the effect of time-variant coupled uplift forces and lateral blast pressures on the vulnerability of reinforced concrete columns when subjected to internal explosions. Yao *et al.* (2016) conducted experimental and numerical investigation on

concrete slabs against blast loading. The results shows that the deflection thickness ratio of RC slab is inversely proportional to the scale distance and the reinforcement ratio. It is observed from the results that reinforcement ratio has great influence on survivability of reinforced concrete slab under blast loading. Zhang and Phillips (2016) presented performance and protection of base isolated structures under blast loading. Supplemental control devices are proposed and it is concluded that it gives satisfactory results. Sami (2017) presented numerical study on the uplift response of reinforced concrete slabs subjected to internal explosions. It is concluded that the ultimate capacity is governed by tensile membrane action and that most critical sections were slab supports. In addition to that, many studies found on detailed experiments and finite element analysis [Ibrahimbegovic (1990), Ibrahimbegovic and Wilson (1991)] using reinforced concrete slab subjected to blast loading [Lu (2009), Xue *et al.* (2013), Dehghani (2018), Lotfi and Zahrai (2018), Zhang *et al.* (2018), Senthil *et al.* (2018), Singhal *et al.* (2018)], however, there are significant shortcomings which is derived from the previous studies.

Based on the detailed literature survey, it is observed that most studies focused on simple experiments on simple slabs, column and bridge elements subjected to blast loading, however numerical investigations on slabs against blast loading has been found to be limited. Also response of the reinforced concrete slab subjected to blast loading under varying mass of TNT has not been studied. None of the author performed simulations on reinforced concrete slab under air blast and surface blast conditions. In the present study, the numerical investigations has been carried out on reinforced concrete slab against blast loading through finite element method. The inelastic behavior of concrete and steel reinforced bar has been incorporated through concrete damage plasticity model and Johnson-cook model respectively and discussed in Section 2. The finite element model have been carried out using commercial tool ABAQUS/CAE is discussed in Section 3. The results obtained from simulations were compared with the experiments available in literature, Li *et al.* (2016). The simulations are carried out against varying standoff distance, mass of TNT, boundary conditions and type of blast and discussed in Section 4. The damage intensity and stresses of reinforced concrete slab were studied in light of deflection, impulsive wave velocity, von-Mises stresses, compression damage of concrete.

2. Constitutive modelling

The inelastic behavior of concrete has been incorporated through concrete damage plasticity model and the model includes compressive and tensile behavior. The elastic and plastic behavior of steel reinforcement bar has been incorporated using Johnson-cook model includes the effect of state of stress, temperature and strain rate and discussed in this section.

2.1 Concrete damaged plasticity model for concrete

In finite element modelling, inelastic behaviour of concrete was defined by using concrete damaged plasticity model (CDP) providing a general capability for modelling concrete and other quasi-brittle materials. The plastic-damage model is a form of plasticity theory in which a plastic-damage variable ' K ' was defined which increases if plastic deformation takes place. Moreover, the plastic-damage variable is limited to a maximum value and the attainment of this value at a point of the solid represents total damage, which can be interpreted as the formation of a macroscopic crack. The variable " K " is non-dimensional and its maximum value is unity. The concrete

Table 1 Compressive damage variables for CDP model

Yield Stress (N/mm ²)	Inelastic Strain	Damage Parameter (d_c)
15.00	0	0
14.32	0.000475	0.045
14.07	0.000575	0.061
13.53	0.000775	0.097
13.25	0.000875	0.116
12.69	0.001075	0.153
12.13	0.001675	0.191
10.60	0.001875	0.293
10.14	0.002875	0.323
7.22	0.003575	0.351

Table 2 Tensile damage variables for CDP model

Yield Stress (N/mm ²)	Cracking Strain	Damage Parameter (d_t)
2.71	0	0
2.30	0.0004	0.211
2.20	0.0008	0.256
2.00	0.0009	0.312
1.91	0.002	0.384

Table 3 Material parameters of concrete, Jankowiak and Lodygowski (2005)

Description	Notations	Numerical value
Modulus of elasticity	E (N/m ²)	19365 x 10 ⁶
Poisson's ratio	ν	0.2
Density	ρ (kg/m ³)	2400
Eccentricity	e	0.1
Dilation angle	Ψ (degree)	38
Bulk modulus	k	0.667
f_{b0}/f_{c0} Ratio	-	1.16

damaged plasticity model is a continuum, plasticity-based, damage model for concrete. The model assumes that the two main failure mechanisms are tensile cracking and compressive crushing of the concrete material. The evolution of the yield surface is controlled by two hardening variables which are linked to failure mechanisms under tension and compression loading, namely ε_c^{pl} and ε_t^{pl} are compressive and tensile equivalent plastic strains, respectively. The damage variables can take values from zero to one, where zero represents the undamaged material and one represents total loss of strength. The stress strain relations under uniaxial compression and tension loading are given by the following equations where E_o is the initial (undamaged) elastic stiffness of the material: $\sigma_t = (1-d_t)E_o(\varepsilon_t - \varepsilon_t^{pl})$ and $\sigma_c = (1-d_c)E_o(\varepsilon_c - \varepsilon_c^{pl})$, where d_t and d_c are tension damage variable and compression damage variable respectively, Senthil *et al.* (2017). The concrete damaged plasticity model parameters such as (d_t) tension and (d_c) compression damage variables are shown

Table 4 Material parameters for steel reinforcing bar, Iqbal *et al.* (2015)

Description	Notations	Numerical value
Modulus of elasticity	E (N/mm ²)	203000
Poisson's ratio	ν	0.33
Density	ρ (Kg/m ³)	7850
Yield Stress constant	A (N/mm ²)	304.330
Strain hardening constant	B (N/mm ²)	422.007
	n	0.345
Viscous effect	C	0.0156
Thermal softening constant	m	0.87
Reference strain rate	$\dot{\epsilon}_0$.0001 s ⁻¹
Melting temperature	θ_{melt} (K)	1800
Transition temperature	$\theta_{transition}$ (K)	293
	D_1	0.1152
	D_2	1.0116
	D_3	-1.7684
	D_4	-0.05279
	D_5	0.5262

in Tables 1 and 2. The compressive strength of concrete was considered 15 MPa and Poisson's ratio of the concrete was assumed equal to 0.20. The parameters for CDP model other than damage variables are shown in Table 3.

2.2 Johnson-Cook model for reinforcement

The flow and fracture behavior of projectile and target material was predicted employing the Johnson-Cook (1985) elasto-viscoplastic material model available in ABAQUS finite element code. The material model is based on the von Mises yield criterion and associated flow rule. It includes the effect of linear thermo-elasticity, yielding, plastic flow, isotropic strain hardening, strain rate hardening, softening due to adiabatic heating and damage. The Johnson and Cook (1985) extended the failure criterion proposed by Hancock and Mackenzie (1976) by incorporating the effect of strain path, strain rate and temperature in the fracture strain expression, in addition to stress triaxiality. The fracture criterion is based on the damage evolution wherein the damage of the material is assumed to occur when the damage parameter, exceeds unity: The strain at failure is assumed to be dependent on a non-dimensional plastic strain rate, a dimensionless pressure-deviatoric stress ratio, (between the mean stress and the equivalent von-Mises stress) and the non-dimensional temperature, defined earlier in the Johnson-Cook hardening model. When material damage occurs, the stress-strain relationship no longer accurately represents the material behavior, ABAQUS (2008). The use of stress-strain relationship beyond ultimate stress introduces a strong mesh dependency based on strain localization i.e., the energy dissipated decreases with a decrease in element size. Hillerborg's fracture energy criterion has been employed in the present study to reduce mesh dependency by considering stress-displacement response after the initiation of damage. The section of the reinforcement is assigned Fe250 steel and the ultimate tensile strength is 250 MPa is approximately equivalent to the ultimate tensile strength proposed by Iqbal *et al.*

(2015) and the material properties of the steel reinforcing bar has been shown in Table 4.

3. Finite element modelling

The finite element model of the reinforced concrete slab was made using ABAQUS/CAE. The length and width of slab was 2.0 and 0.8 m respectively exactly proposed by Li *et al.* (2016), see

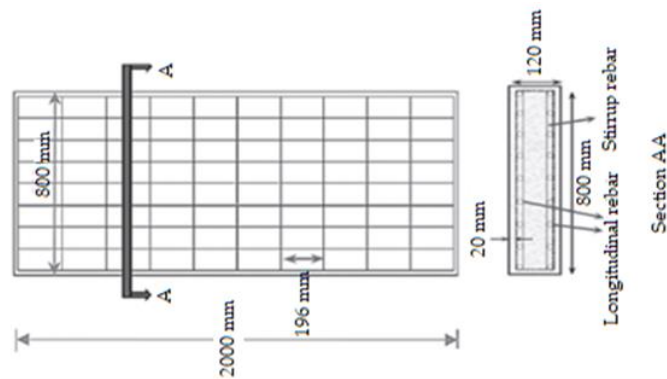
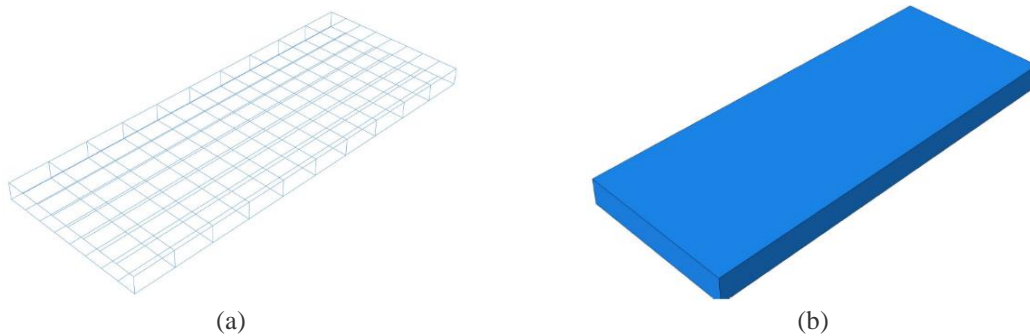


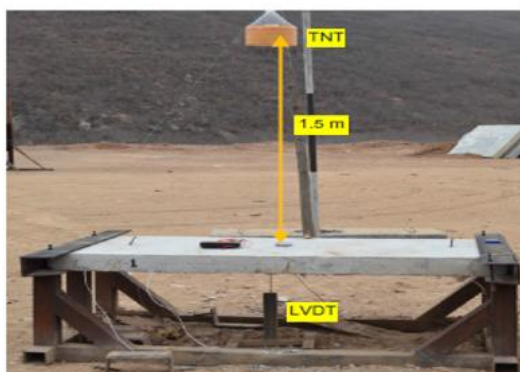
Fig. 1 Schematic of reinforced concrete slab, Li *et al.* (2016)



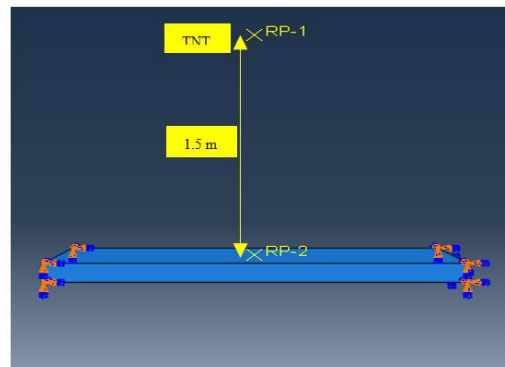
(a)

(b)

Fig. 2 Modelling of (a) reinforcement and (b) concrete



(a)



(b)

Fig. 3 Picture showing (a) Experimental setup (Li *et al.* 2006) and (b) Simulation

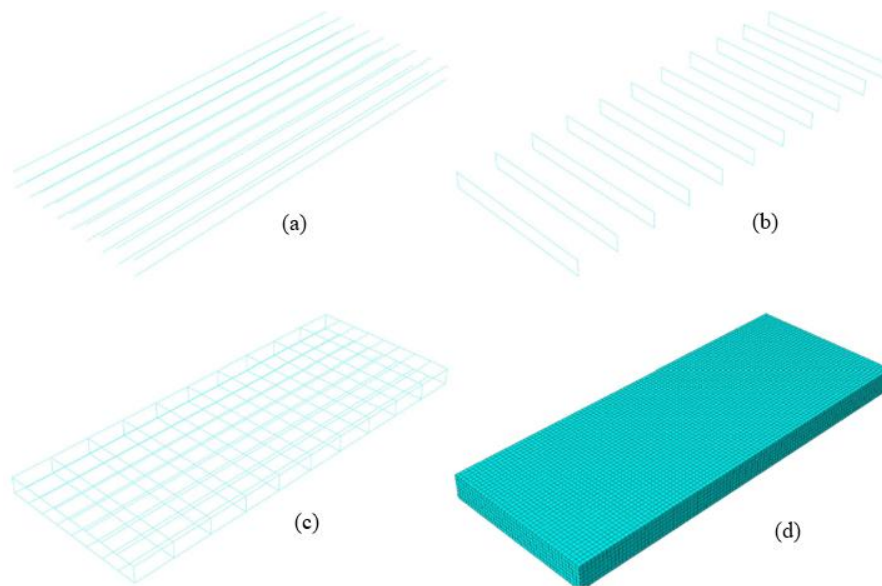


Fig. 4 Finite element modelling of (a) main reinforcement (b) stirrups (c) combination of main reinforcement and stirrups and (d) concrete

Fig. 1. The thickness of slab was 120 mm and clear cover is 20 mm on both the side of slab. The top and bottom steel reinforcement of main bar was 12 mm diameter placed at 95 mm center to centre distance. The size of stirrup reinforcement in slab was considered as 10 mm diameter placed at 196 mm centre to centre distance on shorter direction, see Fig. 1. The geometry of the concrete and steel reinforcement was modelled as solid deformable body, Fig. 2(a)-2(b). The interaction between concrete and steel was modelled using the tie constraint option available in ABAQUS/CAE wherein the concrete was assumed as host region and the steel as embedded region. The constitutive and fracture behavior of steel and concrete have been predicted using Johnson-Cook and Concrete damaged plasticity model respectively available in ABAQUS. The origin of blast considered against 1.5 m from the exterior top surface of slab and 8 kg mass of TNT.

Fig. 3(a) showing the slab placed on a steel frame with the height of 600 mm above the ground, (Li *et al.* 2016). The combined model of slab has been shown in Fig. 3(b) and the rotational and translational motion of the slab was restricted to depict rigid supports at the ends. The blast load was incorporated using interaction module available in ABAQUS. The surface blast load was created using CONWEP definition and the surface blast was consigned with help of two reference point (RP-1 and RP-2) which is assigned based on standoff distance from point of response. For surface blast two reference points were created and in case of air blast loading, one reference point was created. For instances, in case of Fig. 3(b), is on surface blast need two reference points to be selected based on standoff distance from centre of slab. The detonator was hexogen (RDX) and the parameters considered for blast load is exactly similar to Li *et al.* (2016). In the present study, the response was measured from the location where maximum damage/deformation/stresses exists otherwise it is chosen at middle of slab. The boundary conditions were defined as clamped at shorter directions and it is proximity of the experiments clamped at its both ends with steel cleats and bolts. This set-up is assumed as an idealized fixed end boundary which prevents slab from

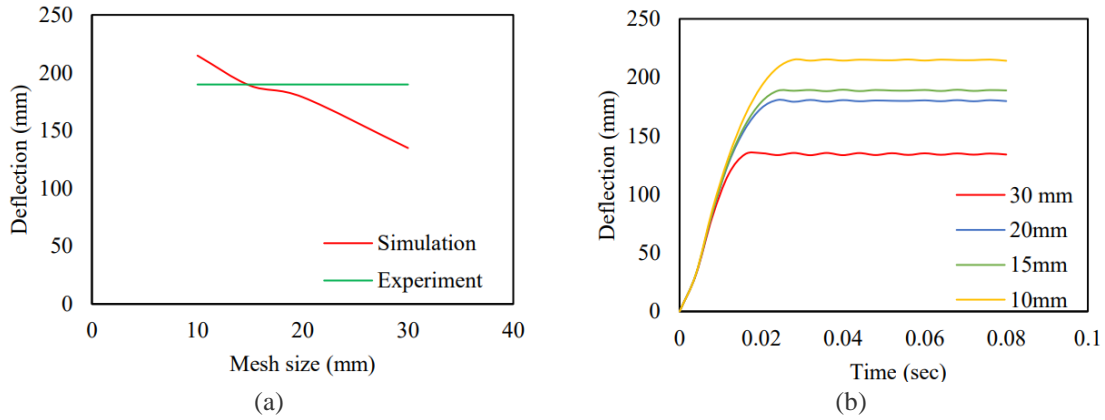


Fig. 5 Deflection of slab function of (a) varying mesh size and (b) time

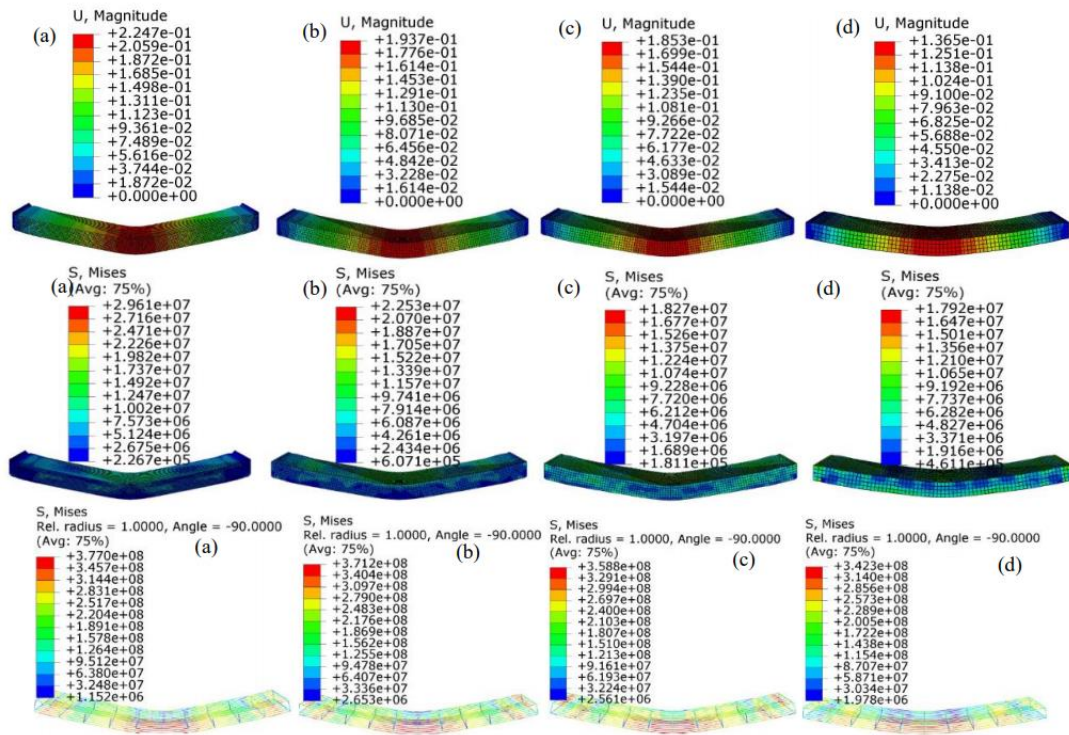


Fig. 6 Von-Mises stresses and deformation of slab against (a) 10 (b) 15 (c) 20 and (d) 30 mm mesh sizes

rebouncing under severe blast loads. The possible explanation regarding design of tests has been given in the manuscript however, a detailed schematic of geometry and the tests conditions were given in Figs. 1 and 2 and Li *et al.* (2016).

The mathematical modelling/constitutive modelling in order to define the damage behaviour of concrete and steel reinforcement has been elaborated in detail in (Iqbal *et al.* 2015 and Senthil *et al.* 2017), however, the damage and the material parameters has been incorporated, please see Tables 1-4. The typical finite element modelling of steel reinforcement and concrete of wall

element has been shown in Fig. 4(a)-4(d). The concrete elements of all the components were meshed using structured elements of 8 noded hexahedral linear brick element and steel reinforcement was meshed with linear beam element. Linear shape functions were used by elements and reduced integration was considered, i.e. per element one integration point. A linear element of type T3D2 (three dimensional two noded truss element) reduced integration. A detailed mesh sensitivity analysis has been carried out to understand the influence of mesh size. The size of element was varied as $0.03 \times 0.03 \times 0.03$ m, $0.02 \times 0.02 \times 0.02$ m, $0.015 \times 0.015 \times 0.015$ m and $0.01 \times 0.01 \times 0.01$ m and corresponding total number of elements were 7236, 24000, 56392 and 192000 respectively.

The predicted deflection of slab was compared with the experimental results, see Fig. 5(a) corresponding to varying mesh size. The predicted deflection at middle of the slab was 215, 190, 179 and 135 mm against 10, 15, 20 and 30 mm mesh size respectively, see Fig. 5(b), whereas the measured deflection through experiment was 190 mm. It is observed that the deflection of slab corresponding element size of 15 and 20 mm was found in good agreement with the experimental results. In addition to that the maximum deflection and Mises stresses in concrete as well as steel reinforcement of varying mesh sizes were compared, see Fig. 6(a)-6(d). It is observed that the Mises stresses in concrete was found to be 29, 22, 18.2 and 17.9 MPa against 10, 15, 20 and 30 mm mesh size respectively. The Mises stresses in steel reinforcement was found to be 377, 371, 358 and 342 MPa against 10, 15, 20 and 30 mm mesh size respectively. Therefore, it is concluded that the mesh size of 20 mm for both reinforcement bar and concrete was found to be suitable for further analysis considering the less computational time and cost. The mesh size of concrete as well as reinforced bar was considered as $20 \times 20 \times 20$ mm. The mesh size 20 mm was assigned, giving a total number of 24000 and 2688 elements for the concrete and reinforced steel bar respectively. The analysis was divided into 20 frames within a time frame of 0.08 second. A CPU time typical simulation for blast event took around 41 hours and 20 minutes.

4. Comparison of experimental and numerical results

The simulations were carried out against 8 kg mass of TNT at a distance of 1.5 from the surface of the slab. The concrete damaged plasticity model has been employed for predicting the material behavior of the concrete, whereas the Johnson-Cook model has been used for predicting the material behavior of steel reinforcement. The three dimensional finite element modelling of the slab including steel reinforcement is discussed in Section 3. The simulated results thus obtained have been compared with the experiments carried out by Li *et al.* (2016) and discussed in this Section.

Fig. 7(a)-7(f) shows the deformed profile of experiments and predicted results in light of displacement, compression damage, tension damage, Mises stress in concrete and steel. It is observed that the maximum deflection obtained numerically is 185 mm, which is very close to the maximum deflection of 190 mm measured throughout the experiment. The predicted deflections are in close agreement to actual experimental results. However, the maximum difference between the actual and predicted deflection was found to be 3%. The predicted concrete compression and tension damage index were 0.336 and 0.385 found closely matching with the input of 0.351 and 0.38, respectively are shown in Table 1. The predicted von-Mises stresses in concrete was 18.2 MPa is almost equivalent to the compressive strength of concrete 15 MPa measured from the experiments. The predicted equivalent von-Mises stresses in the reinforcement bar was 525 MPa

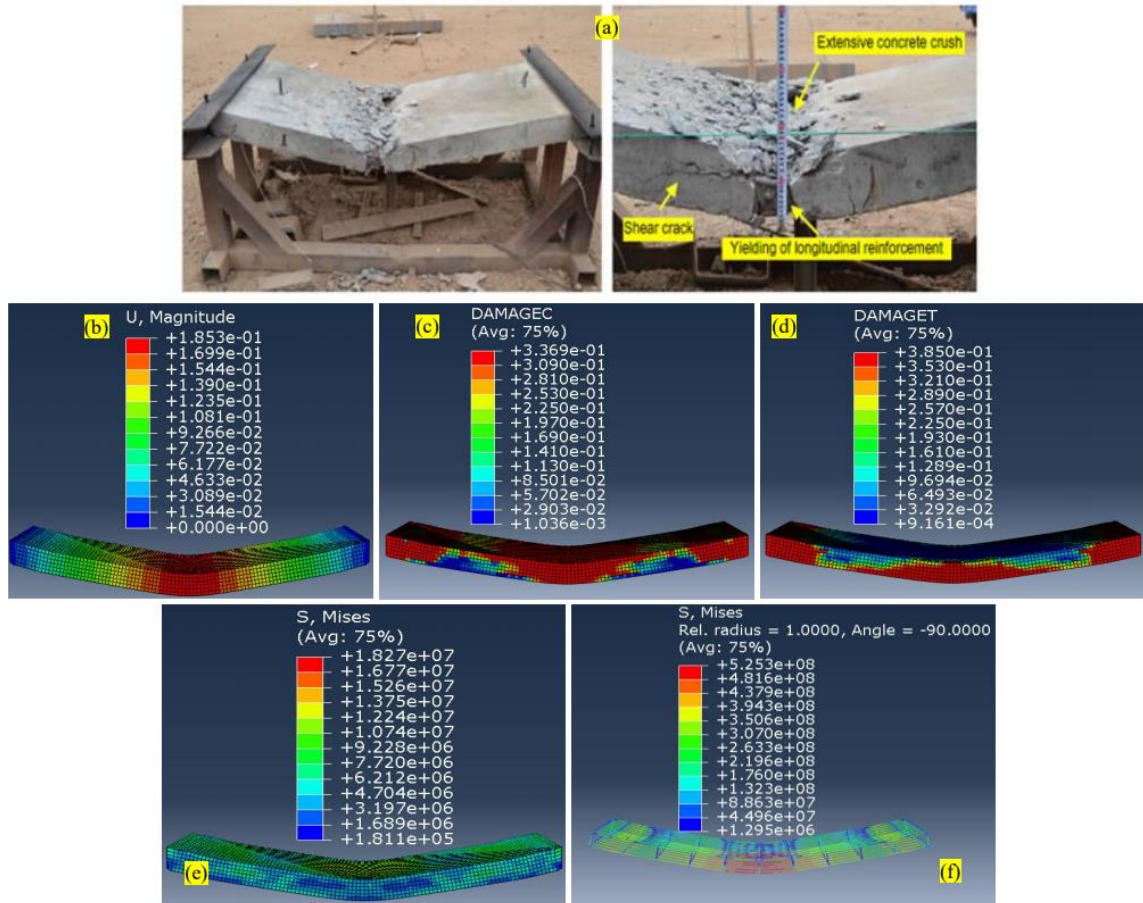


Fig. 7 Deformed profile of (a) experiments and predicted results of (b) displacement (c) compression damage (d) tension damage (e) Mises stress in concrete and (f) Mises stress in steel

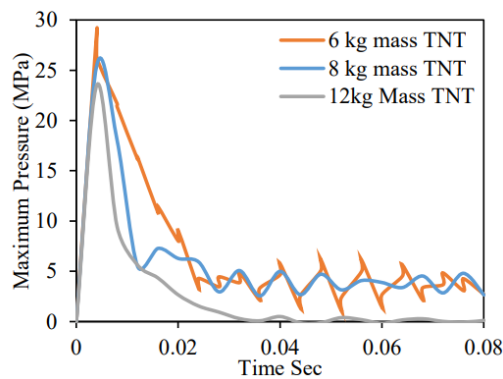


Fig. 8 Pressure-Impulse waves against blast load by varying mass of TNT at a distance of 1.5 m

which is close to the true stress measured from the experiment, Iqbal *et al.* (2015). The actual and predicted deformation of the slab as a result of failure has been compared and almost exact pattern

of deformation has been predicted through numerical simulations. For further understanding, the Pressure-Impulse waves were obtained against the blast load by varying mass of TNT at a distance of 1.5 m using CONWEP command available in ABAQUS is shown in Fig. 8. The maximum impulsive pressure generated through simulation was 29, 25 and 24 MPa, against 6, 8 and 12 kg mass of TNT, respectively.

5. Results and discussion

Three-dimensional finite element analysis has been carried out in order to study the response of reinforced concrete slab against blast loading using ABAQUS/CAE. The simulations were carried out against varying standoff distance, mass of TNT and different support condition. Also the response of slab have been studied against surface blast as well as air blast loading. The response of structural elements were observed in terms of deflection, impulsive velocity, von-Mises stresses and compression damage therein were presented and discussed.

5.1 Effect of varying mass of TNT

The simulations were carried out against varying mass of TNT at constant standoff of distance, i.e. 1.5 m. The response of 120 mm thick slab was studied against varying mass of TNT and the mass considered as 6.0, 8.0 and 12 kg. The behaviour of reinforced concrete slab in terms of deflection, impulse velocity, Mises stresses in concrete and steel bar and compression damage against varying mass of TNT is shown in Figs. 9 and 10.

The displacement of slab against blast load of varying mass TNT originated at 1.5 m from the surface is shown in Fig. 9(a-i)-(c-i). The unit of the displacement contours was "meter". The maximum deflection was found to be 307, 185 and 120 mm against 12, 6 and 8 kg mass TNT respectively. It is observed that the deflection in the slab was found to be increased by 156% when the mass of TNT increased from 6 to 12 kg. It is concluded that for every increase of 33.33% weight of TNT, the deflection increases by 52% for a standoff distance of 1.5m. The maximum deflection on slab was about 307 mm against mass of 12 kg TNT and it is found to be more vulnerable. The deflection of slab against 12 kg mass was found increased to 39 and 60% as compared to the deflection of slab by 6 and 8 kg mass TNT respectively. It is also clearly seen that the deflection reaches its peak value within 0.02 seconds i.e., from the time of detonation, see Fig. 10(a).

The impulse velocity due to the blast due to varying mass of TNT has been shown in Fig. 9(a-ii)-(c-ii). The unit of the velocity contours was "meter per second". The maximum impulse velocity 11, 13.2 and 17.9 m/s against 6, 8 and 12 kg mass TNT respectively. It is observed that the impulsive velocity was found to increase with increase in mass of TNT. The impulse velocity against 12 kg mass was found increased to 61 and 73% as compared to the velocity of 6 and 8 kg mass TNT respectively. As it was clearly seen that velocity reaches its maximum within 0.02 seconds after which it drops to almost zero, see Fig. 10(b).

The compression damage index of reinforced concrete slab against blast load of varying mass TNT is shown in Fig. 9(a-iii)-(c-iii). The compression damage contours described by unit less factor. The maximum damage due to compression was found to be 0.336 for against all chosen mass of TNT. The compression damage parameter was considered maximum of 0.351 in the present study. It is observed that the compression damage in the slab was found to reach maximum

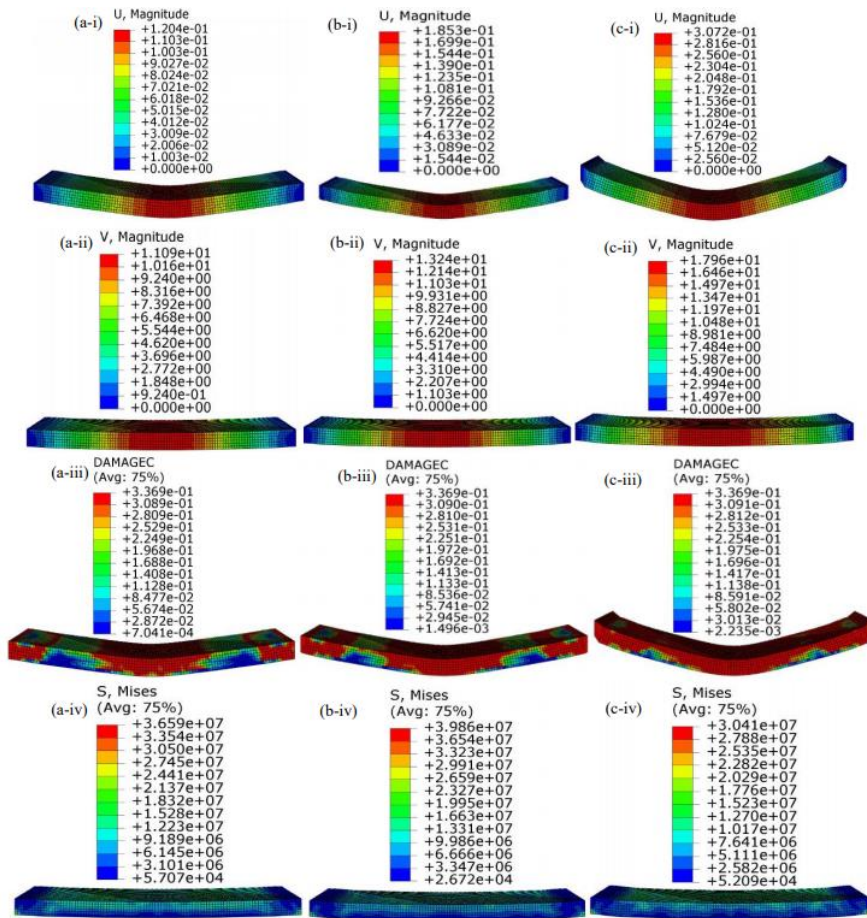


Fig. 9 (i) Deflection of slab (ii) impulse velocity (iii) compression damage (iv) Mises stresses in concrete and steel bar and against (a) 6 (b) 8 and (c) 12 kg mass TNT

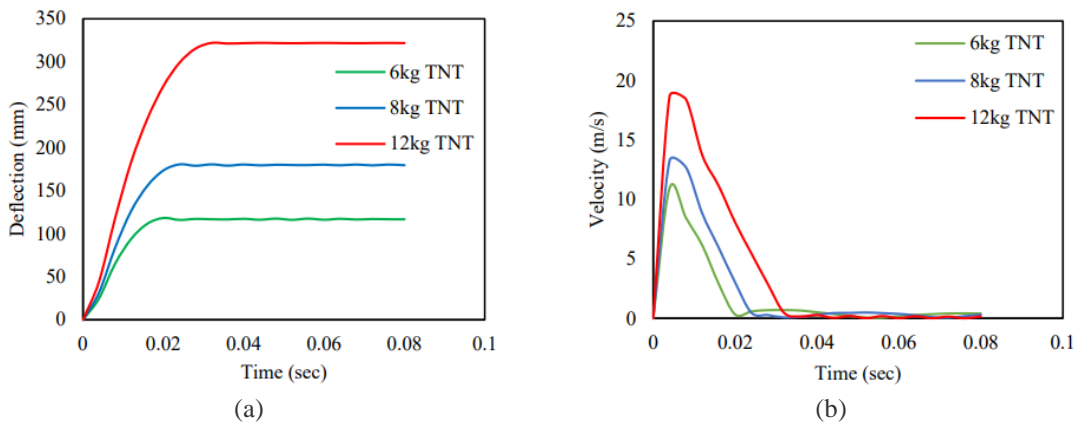


Fig. 10 Response in terms of (a) deflection and (b) impulse velocity function of time at varying mass of TNT against 6 kg mass TNT. Also it was observed that the damage intensity was found increasing with

increase of mass of TNT. From this observation, it is concluded that the slab was found to be more vulnerable against 6 kg mass of TNT and the slab may be safe if the mass of TNT below 6 kg.

The von-Mises stresses in concrete against blast load of varying mass TNT is shown in Fig. 9(a-iv)-(c-iv). The unit of the von-Mises stress in the contours is “N/m²”. At 0.004 second time step, the maximum von-Mises stress at the concrete was found to be 36, 39.8 and 30.4 MPa for 6, 8 and 12 kg mass TNT respectively. However, it is observed that the stress in concrete was found to be almost 20 MPa after 0.004 second time step. The highest stress is at 0.004 second, it may be due to the highest impulse velocity during the detonation of blast. Also, it is observed that the stress in concrete was found to be increased when the mass of TNT increased from 6 to 8 kg, whereas the trend is reverse when the mass of TNT increased from 8 to 12 kg. The von-Mises stresses in steel reinforcement against blast load of varying mass of TNT is shown in Fig. 9(a-v)-(c-v). The von-Mises stress at the steel reinforced bar was found to be 494, 525 and 555 MPa for 6, 8 and 12 kg mass TNT respectively. It is observed that the stress was found to increase with increase in mass of TNT. Therefore, it is concluded that the steel reinforcement was found observing the stresses efficiently then the concrete when the mass of TNT is significantly higher. Therefore, it is concluded that the maximum stress in the concrete was found to be in the range of 15 to 20 N/mm² and is almost constant against 6, 8 and 12 kg charge weight.

5.2 Effect of varying standoff distance

The simulations were carried out against varying standoff distance at constant mass of TNT, i.e. 8 kg. The response of reinforced concrete slab was studied against varying standoff distance and the standoff distance considered as 1.5, 2.0, 5.0 and 8 m. The behaviour of reinforced concrete slab in terms of deflection, impulse velocity, Mises stresses in concrete and steel bar and compression damage against varying standoff distance is shown in Figs. 11 and 12.

The displacement of slab against blast load of by 8 kg mass TNT originated at 1.5, 2, 5 and 8 m from the surface is shown in Fig. 11(a-i)-(d-i). The maximum deflection was found to be 185, 87.9, 6.4 and 0.33 mm against 1.5, 2.0, 5.0 and 8 m standoff distance respectively. The maximum deflection on slab was about 185 mm against 1.5 m distance and it is found to be more vulnerable. The deflection of slab against 1.5 m standoff distance was found decreased to 47, 3.4 and 0.5% as compared to the deflection of slab by 2, 5 and 8 m respectively. It is observed that given slab doesn't experience damage against 5 and 8 m standoff distance. It is also clearly seen that the deflection reaches its peak value within 0.02 seconds i.e., from the time of detonation, see Fig. 12(a).

The impulse velocity due to blast at varying standoff distance has been shown in Fig. 11(a-ii)-(d-ii). The maximum impulse velocity was found to be 13, 9.7, 2.83 and 1.04 m/s against 1.5, 2.0, 5.0 and 8 m standoff distance respectively. It is observed that the impulsive velocity was found to decrease with increase of standoff distance. The reason may be due to the fact that the intensity of impulse wave generated by blast tend to be weaker as standoff distance increases. The impulse velocity against 1.5 m standoff distance was found decreased to 75, 22 and 8% as compared to 2, 5 and 8 m distance from the surface, respectively. As it was clearly seen that velocity reaches its maximum within 0.02 seconds after which it is drops to almost zero, see Fig. 12(b). It is also observed that the maximum velocity reaches the slab at 0.004, 0.005, 0.008 and 0.02 seconds by 1.5, 2, 5 and 8 m standoff distance, respectively.

The compression damage of slab against blast load of 8 kg mass of TNT at varying standoff distance is shown in Fig. 11(a-iii)-(d-iii). The maximum compression damage was observed 0.336

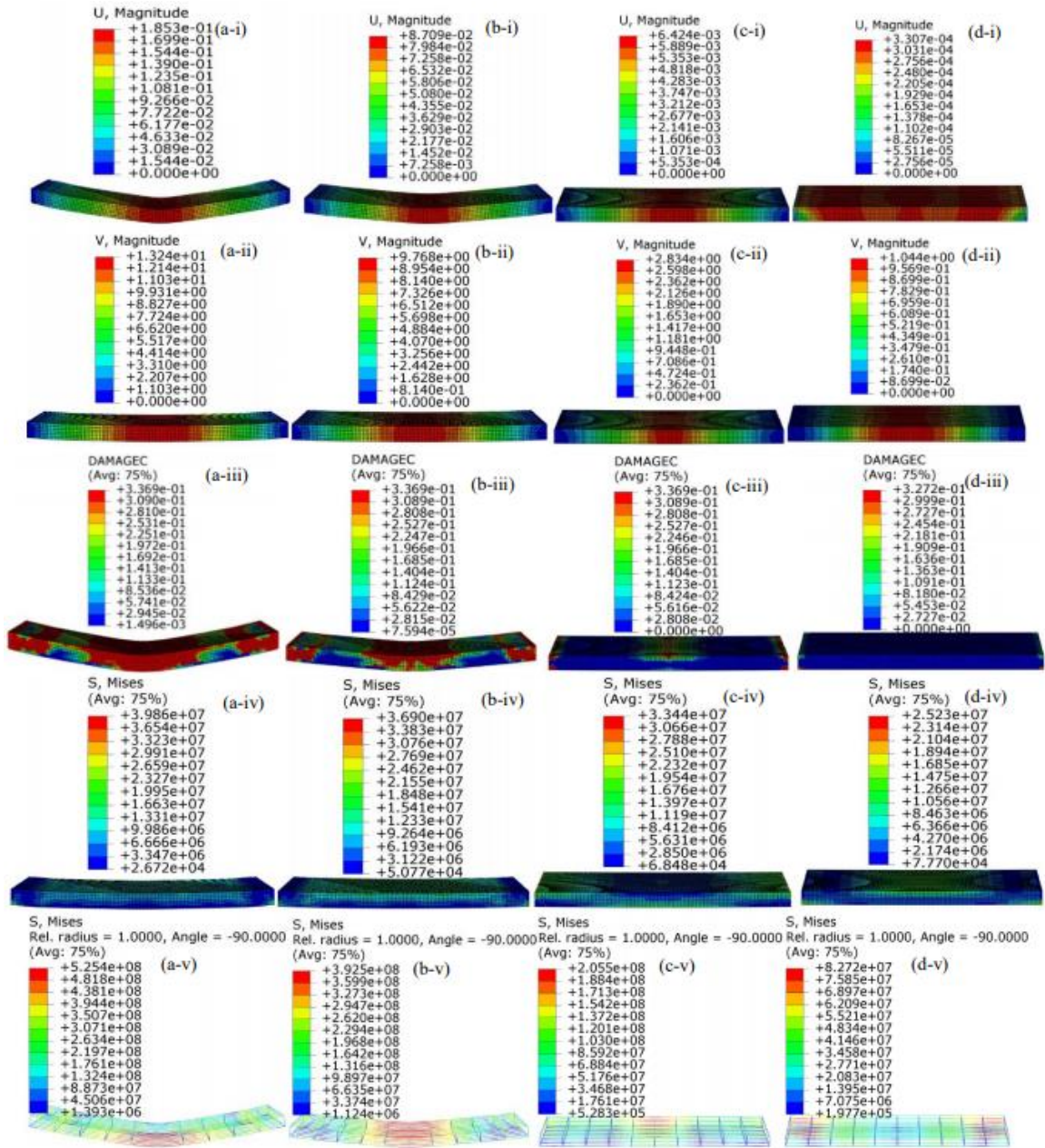


Fig. 11 (i) Deflection of slab (ii) impulse velocity (iii) compression damage and Mises stresses in (iv) concrete and (v) steel at (a) 1.5 (b) 2 (c) 5 and (d) 8 m standoff distance

against 1.5, 2 and 5 m standoff distance, however the damage was found to be insignificant i.e., 0.327, against 8 m distance. Also it was observed that the damage intensity was found decreasing with increase of standoff distance. Therefore, it is observed that the compression damage index in slab was found to be vulnerable against 1.5, 2 and 5 m standoff distance whereas the slab was safe

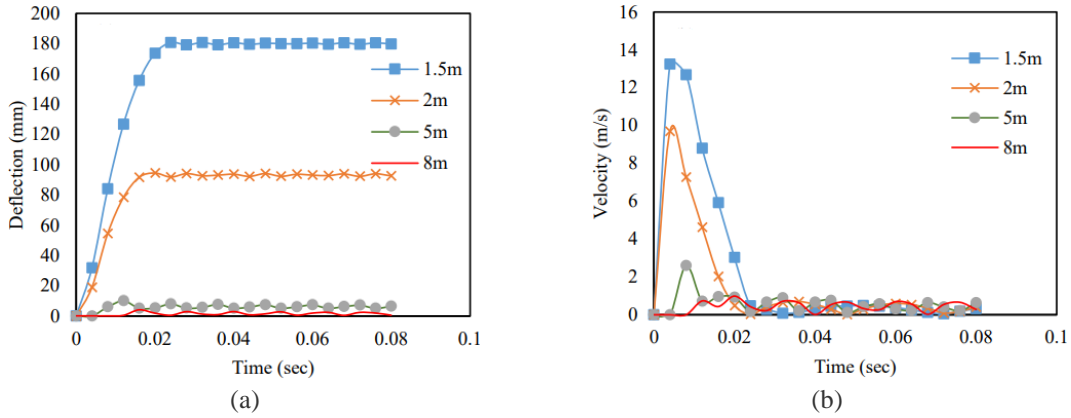


Fig. 12 Response in terms of (a) deflection and (b) impulse velocity function of time at varying standoff distance

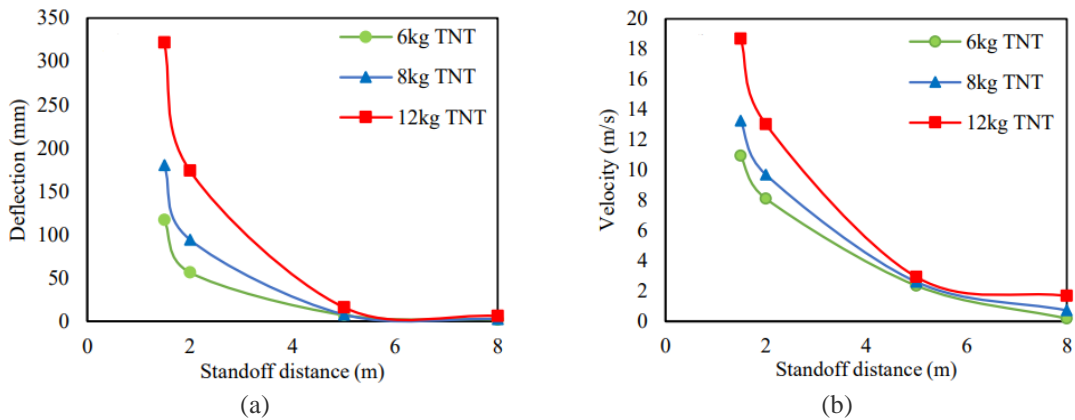


Fig. 13 Response of slab in terms of (a) deflection and (b) impulse velocity against varying mass of TNT function of varying standoff distance

against 8 m standoff distance. Therefore, it is concluded that the slab was found to be more vulnerable upto the standoff distance of 5 m and thereafter slab found safe at given mass of TNT 8 kg.

The von-Mises stresses in concrete against blast load of 8 kg mass of TNT at varying standoff distance is shown in Fig. 11(a-iv)-(d-iv). At 0.004 second time step, the maximum von-Mises stress at the concrete was found to be 39.8, 36.9, 33.4 and 25.2 MPa for 1.5, 2, 5 and 8 m standoff distance respectively. However, it is observed that the stress in concrete was found to be almost in the range of 21-15 MPa after 0.004 second time step. The slab experienced highest stress at 0.004 second for 1.5 and 2 m standoff distance whereas the same was found at 0.016 second for 5 and 8 m distance. Also, it is observed that the stress in concrete was found to be decreased when the standoff distance increase from 1.5 to 8 m. The von-Mises stresses in steel reinforcement against blast load at varying standoff distance is shown in Fig. 11(a-v)-(d-v). The von-Mises stress at the steel reinforced bar was found to be 525, 392, 205 and 82 MPa for 1.5, 2, 5 and 8 m standoff distance respectively. It is observed that the stress was found to decrease significantly with increase in standoff distance. Therefore, it is concluded that the concrete was found observing the

stresses efficiently than the steel when the standoff distance is significantly higher.

5.3 Effect of varying standoff distance and mass of TNT

The influence of varying mass of TNT and varying standoff distance has been studied in the previous Section 5.1 and 5.2 respectively. In the present section, the effect of combination of varying standoff distance as well as varying mass of TNT has been discussed. The simulations were carried out against varying standoff distance i.e., 1.5, 2, 5 and 8 m at varying mass of TNT, i.e., 6, 8 and 12 kg. The behaviour of reinforced concrete slab in terms of deflection and impulse velocity is shown in Fig. 13(a)-13(b).

It was observed from the Fig. 13(a) that the standoff distance increases the maximum deflection in slab was found decreases significantly. At 1.5 m standoff distance, the maximum deflection was found to be 322, 185 and 118 mm against 12, 8 and 6 kg mass of TNT respectively. At 2 m standoff distance, the maximum deflection was found to be 174, 94, and 56 mm against 12, 8 and 6 kg mass of standoff distance respectively. At 5 and 8 m standoff distance, the deflection in slab

was found to be insignificant, even though the mass of TNT is very high. This is clearly seen from the Fig. 13(a) that maximum deflection found almost zero against all given charge weight. This is due to the fact that the intensity of impulse wave tend to be weaker as standoff distance increases. Therefore, it is concluded that this phenomenon may be utilised in designing of important structures like nuclear containment, airport building, security station, ministry and hospital building which are prone to terrorist attacks by keeping the important structure away from the boundary up to the distance at which blast effect is minimum.

It was observed from the Fig. 13(b) that the standoff distance increases the maximum impulse velocity generated in slab was found decreases significantly. At 1.5 m standoff distance, the maximum velocity was found to be 18.6, 13.2 and 10.9 m/s against 12, 8 and 6 kg mass of TNT respectively. At 2 m standoff distance, the maximum impulse velocity was found to be 13, 9.7 and 8.1 m/s against 12, 8 and 6 kg mass of standoff distance respectively. At 5 and 8 m standoff distance, the velocity of impulse was found to be insignificant, i.e. 3 m/s irrespective of charge weight. It is observed that when the standoff distance increases and weight of TNT decreases, the maximum impulse velocity found decreases, this implies that velocity is inversely proportional to standoff distance and directly proportional to charge weight.

5.4 Effect of varying boundary condition

Due to non-uniformity in buildings supports and structures one could find the different end boundary conditions. The support conditions of reinforced concrete slab was considered based on the provisions made by Indian standard practices, IS 456:2000. The behaviour of reinforced concrete slab in terms of deflection, impulse velocity and Mises stresses in concrete element against varying standoff distance is shown in Figs. 14-18.

The deflection of slab having different boundary conditions function of time is shown in Fig. 14. It was observed that maximum deflection reaches its peak value within the time step 0.02 seconds for all the boundary conditions except slab with three adjacent edge discontinuous. The deflection of slab having three adjacent edge discontinuous found increased upto time step 0.06 second, thereafter the deflection of slab is constant. The maximum deflection in slab of different boundary conditions such as all edges continuous, two long adjacent edges discontinuous, two

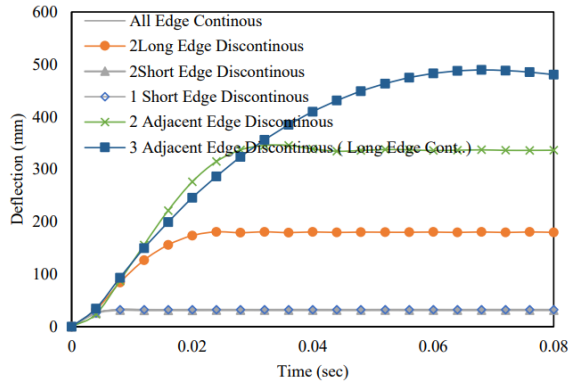


Fig. 14 Deflection of slab at different boundary conditions function of time

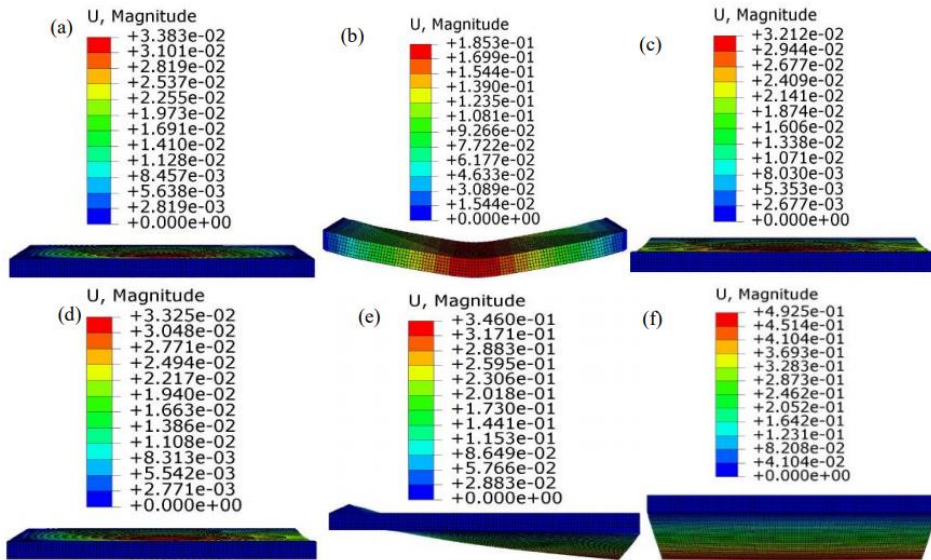


Fig. 15 Maximum deflection in slab having (a) all edges continuous (b) 2 long adjacent edges discontinuous (c) 2 short edge discontinuous (d) 1 short edge discontinuous (e) 2 adjacent edges discontinuous and (f) 3 adjacent edge discontinuous end conditions

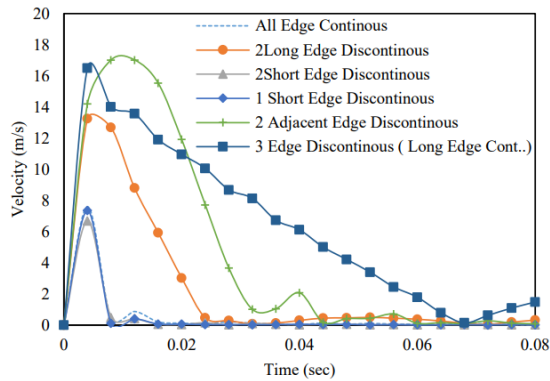


Fig. 16 Impulse velocity in slab having different end conditions function of time

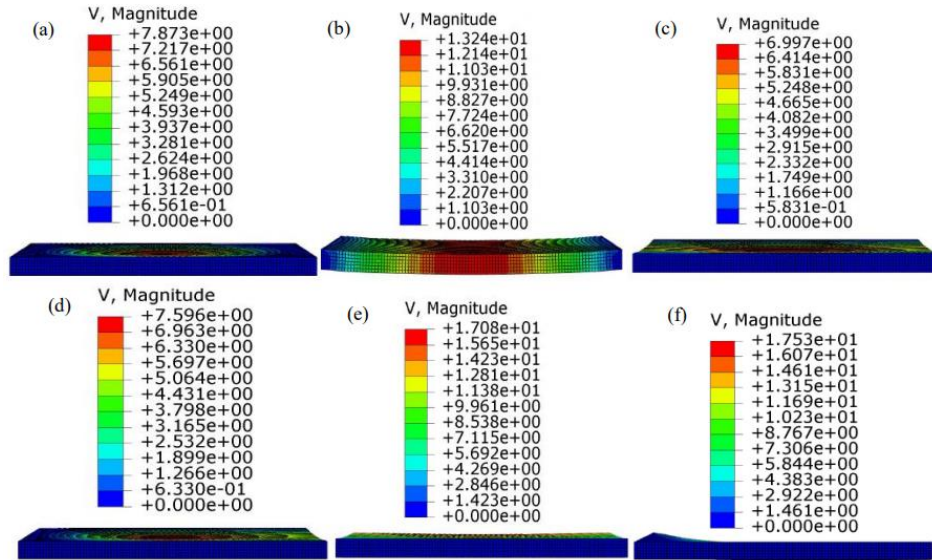


Fig. 17 Maximum impulse velocity in slab having (a) all edges continuous (b) 2 long adjacent edges discontinuous (c) 2 short edge discontinuous (d) 1 short edge discontinuous (e) 2 adjacent edges discontinuous and (f) 3 adjacent edge discontinuous end conditions

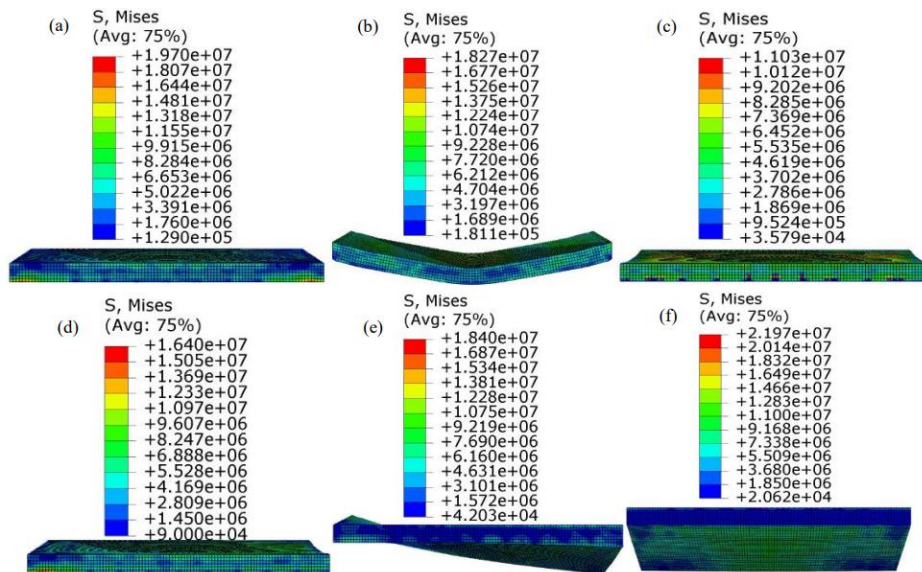


Fig. 18 Mises stresses in slab having (a) all edges continuous (b) 2 long adjacent edges discontinuous (c) 2 short edge discontinuous (d) 1 short edge discontinuous (e) 2 adjacent edges discontinuous and (f) 3 adjacent edge discontinuous end conditions at 0.08 second

short edge discontinuous, one short edge discontinuous, two adjacent edges discontinuous and three long edge discontinuous were shown in Fig. 15. The maximum deflection of slab subjected to all edges continuous, two long adjacent edges discontinuous, two short edge discontinuous, one short edge discontinuous, two adjacent edges discontinuous and three long edge discontinuous was

observed 33.8, 185, 32, 33, 346 and 495 mm respectively. The maximum deflection was observed when the slab subjected to three edges discontinuous and the minimum deflection when the slab subjected to two short edges discontinuous. However the deflection of slab having boundary of all edges continuous, two short edge discontinuous and one short edge discontinuous was found to be almost same, 33 mm.

The velocity of impulse generated due to blast load and the response of slab having different boundary conditions function of time is shown in Fig. 16. It was observed that maximum deflection reaches its peak value within the time step 0.004 second for all the boundary conditions except slab with two adjacent edge discontinuous. The maximum velocity generated against slab having three adjacent edge discontinuous at 0.008 second time step. The maximum velocity which are generated by slab of different boundary conditions such as all edges continuous, two long adjacent edges discontinuous, two short edge discontinuous, one short edge discontinuous, two adjacent edges discontinuous and three long edge discontinuous were shown in Fig. 17. The maximum velocity generated by slab subjected to all edges continuous, two long adjacent edges discontinuous, two short edge discontinuous, one short edge discontinuous, two adjacent edges discontinuous and three long edge discontinuous was observed 7.87, 13.2, 6.99, 7.59, 17.08 and 17.53 m/s respectively. The maximum velocity was observed when the slab subjected to three edges discontinuous and the minimum deflection when the slab subjected to two short edges discontinuous. However the velocity generated by slab having boundary of all edges continuous, two short edge discontinuous and one short edge discontinuous was found to be almost same, 7 m/s. It is observed that the boundary conditions of slabs affects the drop of impulse velocity after peak. The drop of velocity was found to be steep for the slab having all edges continuous, two short edge discontinuous and one short edge discontinuous and the time covered to zero velocity is 0.04 second. However, the drop of velocity is almost linear for the slab having two short edge discontinuous, two adjacent edges discontinuous and three long edge discontinuous and the time covered to zero velocity is 0.025, 0.045 and 0.068 respectively.

The von-Mises stresses in concrete against blast load by 8 kg mass TNT at 1.5 m standoff distance and the response of slab having different boundary conditions at 0.08 second is shown in Fig. 18. It is observed that maximum stress reaches its peak value within 0.008 second irrespective of the boundary conditions. At 0.08 second, the maximum stress was observed when the slab having three adjacent edges discontinuous and the minimum stress was observed when the slab is discontinuous on two short edges discontinuous. The maximum stress developed by slab having all edges continuous, two long adjacent edges discontinuous, two short edge discontinuous, one short edge discontinuous, two adjacent edges discontinuous and three long edge discontinuous was observed 19.7, 18.2, 11.0, 16.4, 18.4 and 21.9 MPa respectively. It is observed that behaviour of slab in terms of von-Mises stress is almost similar for all edge conditions except two short edge discontinuous. The stress developed in the slab having two short edge discontinuous was found decreased by almost 30-50% as compared to other end conditions considered in the present study. It is also observed that the deflection, impulse velocity and stress in slab having two short edge discontinuous end conditions were 32 mm, 6.99 m/s and 11.03 MPa respectively and it seems to be the best boundary conditions among the chosen configurations. Therefore, it is concluded that the slab with two short edge discontinuous may be utilised in designing of important structures.

5.5 Effect of varying the type of blast

The influence of surface blast on reinforced concrete slab has been studied in the previous

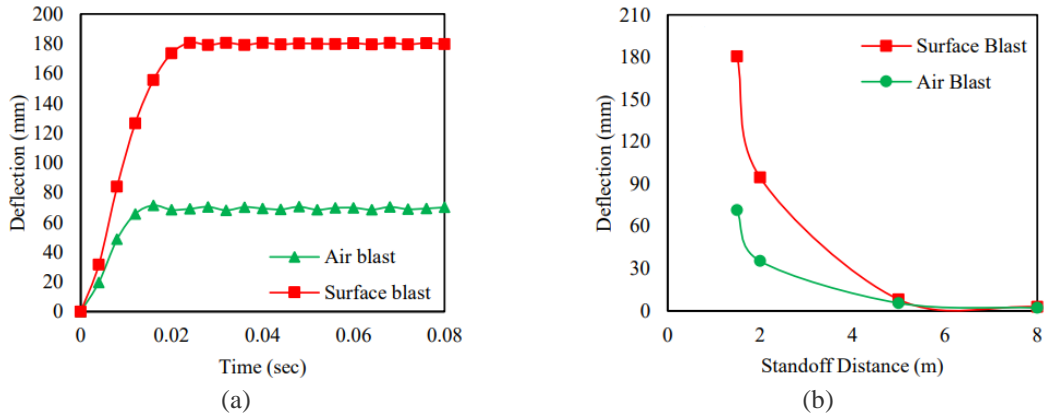


Fig. 19 Deflection of slab due to surface and air blast with (a) function of time and (b) function of standoff distance

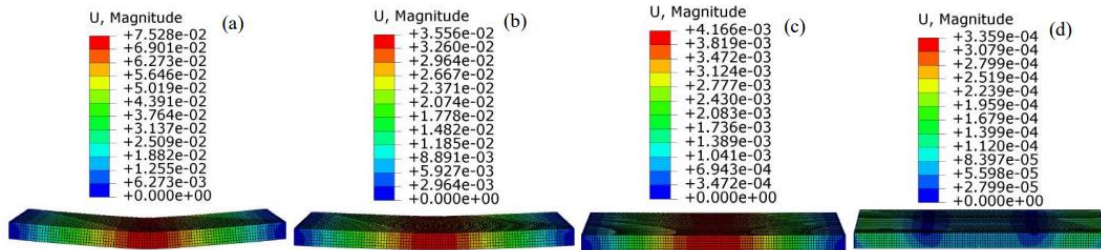


Fig. 20 Deflection of slab due to air blast against (a) 1.5 (b) 2 (c) 5 and (d) 8 m standoff distance

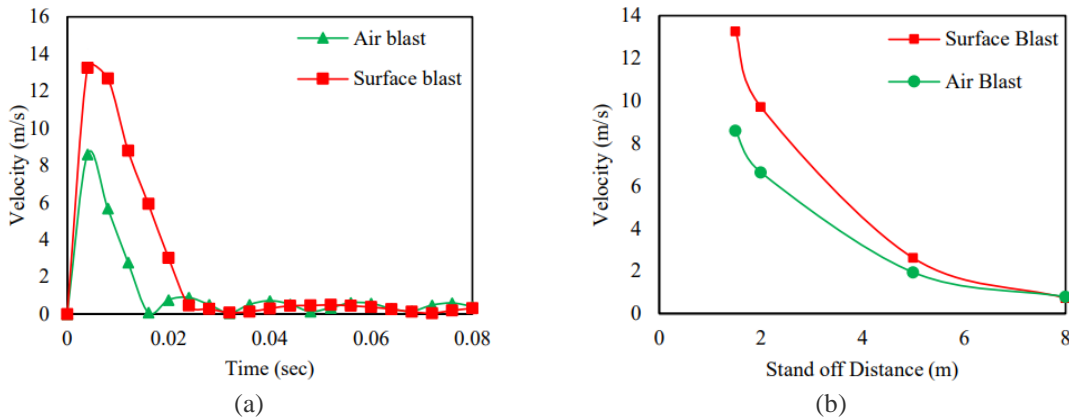


Fig. 21 Impulse velocity at concrete element due to surface and air blast with (a) function of time and (b) function of standoff distance

Section 5.1-5.4. In the present section, the response of reinforced concrete slab against air blast has been studied and compared with the surface blast load by 1.5 kg mass of TNT at varying standoff distance. The behaviour of reinforced concrete slab in terms of deflection and impulse velocity, von-Mises stresses in concrete is shown in Figs. 19-23.

The deflection of slab function of time against air and surface blast by 8 kg mass TNT at 1.5 m

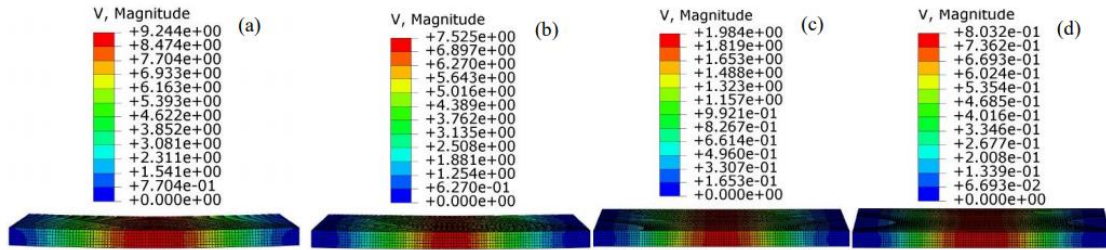


Fig. 22 Impulse velocity at concrete element due to air blast against (a) 1.5 (b) 2 (c) 5 and (d) 8 m standoff distance

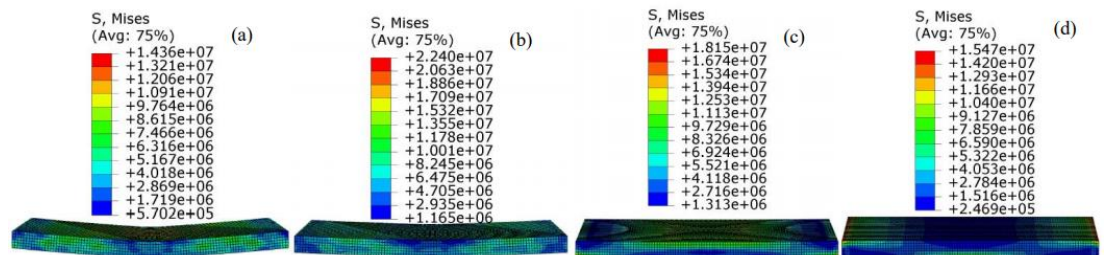


Fig. 23 Mises stresses in concrete against (a) 1.5 (b) 2 (c) 5 and (d) 8 m standoff distance at 0.08 seconds

standoff distance is shown in Fig. 19(a). The deflection of slab was found to be 185 and 68 mm by surface blast and air blast respectively. For the given charge weight and standoff distance the deflection due to air blast decreases by 63% as compared to the surface blast. It was clearly seen from the deformed shape of slab that bending is more in surface blast due to which more stresses are developed. This is due to the fact that in surface blast epicentre is located on the surface of the structure under consideration while in the air blast epicentre is located in the air. It is clearly seen that the deflection reaches its peak value in less than 0.02 second. This implies that the peak attainment is same whether the blast is on surface or in the air.

The deflection of slab function of standoff distance by air blast and surface blast by 8 kg mass TNT is shown in Fig. 19(b). At surface blast, the maximum deflection was found to be 185, 87.9, 6.4 and 0.33 mm against 1.5, 2.0, 5.0 and 8 m standoff distance respectively. At air blast, the maximum deflection was found to be 75.2, 35.5, 4.1 and 0.33 mm against 1.5, 2.0, 5.0 and 8 m standoff distance respectively, see Fig. 20. It is observed that the deflection decreased by 53%, 88%, 92% when standoff distance increases from 1.5 to 2m, 2m to 5m and 5 to 8m respectively. It is clearly seen from the Fig. 19(b) that as the standoff increases beyond 5 m, the deflection of slab for both surface blast as well as air blast converges and is almost equal to zero. This implies that for greater standoff distance surface blast and air blast phenomenon are quiet similar. It is concluded that surface blast produce more damage to the structure as compared to air blast for the same standoff distance but as the standoff distance increases the intensity of damage caused by both the blast are similar.

The impulse velocity developed by slab against air and surface blast by 8 kg mass TNT at 1.5 m standoff distance is shown in Fig. 21(a). The velocity of impulse was found to be 13.2 and 8.59 m/s by surface blast and air blast respectively. It was observed that velocity wave generated due to impulse is maximum for surface blast. It is clearly seen that the velocity reaches its peak value in less than 0.02 second. For the given charge weight and standoff distance the impulse velocity due

to air blast decreases by 35% as compared to the surface blast. This is due to the fact that during air blast epicentre is located just at the point where blast is occurring whereas in case of air blast, the epicentre is away from the surface.

The velocity function of standoff distance by air blast and surface blast by 8 kg mass TNT is shown in Fig. 21(b). Due to surface blast, the maximum impulse velocity was found to be 13, 9.7, 2.83 and 1.04 m/s against 1.5, 2.0, 5.0 and 8 m standoff distance respectively. Due to air blast, the maximum impulse velocity was found to be 9.24, 7.52, 1.98 and 0.8 m/s against 1.5, 2.0, 5.0 and 8 m standoff distance respectively, see Fig. 22. It is observed that the velocity decreases by 19%, 74%, 60% when standoff distance increases from 1.5 to 2m, 2m to 5m and 5 to 8m respectively. It is clearly seen from the Fig. 21(b) that as the standoff increases beyond 5 m, the impulse velocity in slab for both surface and air blast is almost equal to zero. This also implies that for greater standoff distance surface and air blast phenomenon are quite similar. Therefore, it is concluded that surface blast produce more damage to the structure as compared to air blast for the same standoff distance however as the standoff distance increases the intensity of damage caused by both the blast are similar. The variation of stress in concrete by air and surface blast for 8kg TNT at 1.5 m standoff distance and the response of slab at 0.08 second by varying standoff distance is shown in Fig. 23. The stress has been reaches its peak value in less than 0.008 seconds.

6. Conclusions

The present study addresses the finite element investigation on the behavior of reinforced concrete slab against blast load. The numerical simulations were carried out using ABAQUS/Explicit finite element model to predict the response of slab and results are compared with the experimental available in literature. The simulations were carried out against varying standoff distance, mass of TNT, boundary conditions and type of blast. The damage mechanism of reinforced concrete slab was studied in terms of deflection, impulse velocity, von-Mises stresses and compression damage of concrete and the following conclusions have been drawn.

- The maximum deflection of slab obtained from simulation was 185 mm which is very close to the experimental results of 190 mm. The actual and predicted deformation of the slab as a result of failure has been compared and almost exact pattern of deformation has been predicted through numerical simulations.

- It is observed that the deflection in the slab was found to be increased by 156% when the mass of TNT increased from 6 to 12 kg. It is concluded that for every increase of 33.33% weight of TNT, the deflection increases by 52%. The velocity of impulse wave was found to be decreased from 17 m/s to 11 m/s when charge weight reduced by 6kg. The maximum stress in the concrete was found to be in the range of 15 to 20 N/mm² and is almost constant for 6, 8 and 12 kg charge weight.

- It was observed that the deflection in the slab at a standoff distance of 2 m, 5 m, 8 m is decreased by 53%, 88% and 92% as compared to standoff distance of 1.5 m respectively. It was concluded from the study that the velocity of impulse wave reduces drastically after 2 m standoff distance.

- It is also observed that the deflection, impulse velocity and stress in slab having two short edge discontinuous end conditions were 32 mm, 6.99 m/s and 11.03 MPa respectively and it seems to be the best boundary conditions among the chosen configurations. The stress developed in the slab having two short edge discontinuous was found to decrease almost 30-50% as compared to

other end conditions considered in the present study. Therefore, it is concluded that the slab with two short edge discontinuous may be utilised in designing of important structures.

- The deflection in slab due to air blast decreases by 63% as compared to surface blast. The impulse velocity due to air blast decreases by 35% as compared to the surface blast. This is due to the fact that during air blast epicentre is located just at the point where blast is occurring whereas in case of air blast, the epicentre is away from the surface.

References

- ABAQUS, (2014), *6.14 Documentation*, Dassault Systemes Simulia Corporation.
- Burrell, R.P., Aoude, H. and Saatcioglu, M. (2015), "Response of SFRC columns under blast loads", *J. Struct. Eng.*, **141**(9), 04014209. [https://doi.org/10.1061/\(ASCE\)ST.1943-541X.0001186](https://doi.org/10.1061/(ASCE)ST.1943-541X.0001186).
- Dehghani, G.A. (2018), "A performance based strategy for design of steel moment frames under blast loading", *Earthq. Struct.*, **15**(2), 155-164. <https://doi.org/10.12989/eas.2018.15.2.155>.
- Etouney, M., Smilowitz, R. and Rittenhouse, T. (1996), "Blast resistant design of commercial buildings", *Pract. Perio. Struct. Des. Const.*, **1**(1), 31-39. [https://doi.org/10.1061/\(ASCE\)1084-0680\(1996\)1:1\(31\)](https://doi.org/10.1061/(ASCE)1084-0680(1996)1:1(31)).
- Ibrahimbegovic, A. (1990), "A novel membrane finite element with an enhanced displacement interpolation", *J. Fin. Element Anal. Des.*, **7**, 167-179. [https://doi.org/10.1016/0168-874X\(90\)90008-3](https://doi.org/10.1016/0168-874X(90)90008-3).
- Ibrahimbegovic, A. and Wilson, E.L. (1991), "Thick shell and solid finite elements with independent rotation fields", *Int. J. Numer. Meth. Eng.*, **31**(7), 1393-1414. <https://doi.org/10.1002/nme.1620310711>.
- Iqbal, M.A., Senthil, K., Bhargava, P. and Gupta, N.K., (2015), "The characterization and ballistic evaluation of mild steel", *Int. J. Impact Eng.*, **78**, 98-113. <https://doi.org/10.1016/j.ijimpeng.2014.12.006>.
- IS 456 (2000), *Plain and Reinforced Concrete—Code of Practice*, Bureau of Indian Standard, New Delhi, India, 1-100.
- Jankowiak, T. and Lodygowski, T. (2005), "Identification of parameters of concrete damage plasticity constitutive model", *Found. Civ. Environ. Eng.*, **6**(1), 53-69.
- Johnson, G.R. and Cook, W.H. (1985), "Fracture characteristics of three metals subjected to various strains, strain rates, temperatures, and pressures", *Eng. Fract. Mech.*, **21**, 31-48. [https://doi.org/10.1016/0013-7944\(85\)90052-9](https://doi.org/10.1016/0013-7944(85)90052-9).
- King, K.W., Wawlawczyk, J.H. and Ozbey, C. (2009), "Retrofit strategies to protect structures from blast loading", *Can. J. Civ. Eng.*, **36**(8), 1345-1355. <https://doi.org/10.1139/L08-058>.
- Li, J., Wu, C., Hao, H., Su, Y. and Liu, Z. (2016), "Blast resistance of concrete slab reinforced with high performance fibre material", *J. Struct. Integ. Mainte.*, **1**(2) 51-59. <https://doi.org/10.1080/24705314.2016.1179496>.
- Liu, H., Torres, D.M., Agrawal, A.K., Yi, Z. and Liu, G. (2015), "Simplified blast-load effects on the column and bent beam of highway bridges", *J. Bridge Eng.*, **20**(10), 06015001. [https://doi.org/10.1061/\(ASCE\)BE.1943-5592.0000738](https://doi.org/10.1061/(ASCE)BE.1943-5592.0000738).
- Lotfi, S. and Zahrai, S.M. (2018), "Blast behavior of steel infill panels with various thickness and stiffener arrangement", *Struct. Eng. Mech.*, **65**(5), 587-600. <https://doi.org/10.12989/sem.2018.65.5.587>.
- Lu, Y. (2009), "Modelling of concrete structures subjected to shock and blast loading: An overview and some recent studies", *Struct. Eng. Mech.*, **32**(2), 235-249. <https://doi.org/10.12989/sem.2009.32.2.235>.
- Ngo, T., Mendis, P., Gupta, A. and Ramsay, J. (2007), "Blast loading and blast effects on structures—An overview", *Elect. J. Struct. Eng.*, **7**(S1), 76-91.
- Ngo, T. and Mendis, P. (2009), "Modelling the dynamic response and failure modes of reinforced concrete structures subjected to blast and impact loading", *Struct. Eng. Mech.*, **32**(2), 269-282. <http://dx.doi.org/10.12989/sem.2009.32.2.269>.
- Osteraas, J.D. (2006), "Murrah building bombing revisited: A qualitative assessment of blast damage and collapse patterns", *J. Perform. Const. Facilities*, **20**(4), 330-335. [https://doi.org/10.1061/\(ASCE\)0887-](https://doi.org/10.1061/(ASCE)0887-)

- 3828(2006)20:4(330).
- Sami, A.K. (2017), "Numerical study on the uplift response of RC slabs subjected to blasts", *J. Perform. Const. Facilities*, **31**(3), 04016105. [https://doi.org/10.1061/\(ASCE\)CF.1943-5509.0000971](https://doi.org/10.1061/(ASCE)CF.1943-5509.0000971).
- Samir, E.A. (2014), "Finite element analysis of reinforced concrete columns under different range of blast loads", *Int. J. Civ. Struct. Eng.*, **5**(2), 155-164.
- Senthil, K., Rupali, S. and Satyanarayanan, K.S. (2017), "Experiments on ductile and non-ductile reinforced concrete frames under static and cyclic loading", *J. Coupled Syst. Multiscale Dyn.*, **5**(1), 38-50. <https://doi.org/10.1166/jcsmd.2017.1118>.
- Senthil, K., Rupali, S. and Kaur, N. (2018a), "The performance of monolithic reinforced concrete structure includes slab, beam and column against blast load", *J. Mater. Eng. Struct.*, **5**(2), 137-151.
- Senthil, K., Gupta, A. and Singh, S.P. (2018b), "Computation of stress-deformation of deep beam with openings using finite element method", *Adv. Concrete Const.*, **6**(3), 245-268. <https://doi.org/10.12989/acc.2018.6.3.245>.
- Singhal, A., Senthil, K. and Shailja, B. (2018), "Influence of boundary condition and mass of TNT on the behaviour of concrete slab under blast loading", *Proceedings of the National Conference on Advanced Structures, Materials and Methodology in Civil Engineering (ASMMCE-2018)*, Jalandhar, India, November.
- Shi, Y., Li, Z.X. and Hao, H. (2009), "Bond slip modelling and its effect on numerical analysis of blast-induced responses of RC columns", *Struct. Eng. Mech.*, **32**(2), 251-267. <http://dx.doi.org/10.12989/sem.2009.32.2.251>.
- Wakchaure, M.R. and Borole, S.T. (2013), "Comparison of maximum stress distribution of long and short side column due to blast loading", *Int. J. Modern Eng. Res.*, **3**(4), 1988-1993.
- Watson, S., Macpherson, W.N., Barton, J.S., Jones, J.D.C., Tyas, A., Pichugin, A.V., Hindle, A., Parkes, W., Dunare, C. and Stevenson, T. (2005), "Investigation of shock waves in explosive blasts using fibre optic pressure sensors", *J. Phys. Conf. Ser.*, **15**, 226-231.
- Wijesundara, L.M.G. and Clublely, S.K. (2015), "Numerical modelling of reinforced concrete columns subject to coupled uplift and shear forces induced by internal explosions", *Struct. Infrastruct. Eng.*, **12**(2), 171-187. <https://doi.org/10.1080/15732479.2014.1002502>.
- Wu, C., Oehlers, D.J., Reberstrost, M., Leach, J. and Whittaker, A.S. (2009), "Blast testing of ultra-high performance fibre and FRP-retrofitted concrete slabs", *Eng. Struct.*, **31**(9), 2060-2069. <https://doi.org/10.1016/j.engstruct.2009.03.020>.
- Xue, X., Yang, X. and Zhang, W. (2013), "Damage analysis of arch dam under blast loading", *Comput. Concrete*, **12**(1), 65-77. <https://doi.org/10.12989/cac.2013.12.1.065>.
- Yao, S., Zhang, D., Chen, X., Lu, F. and Wang, W. (2016), "Experimental and numerical study on the dynamic response of RC slabs under blast loading", *Eng. Fail. Anal.*, **66**, 120-129. <https://doi.org/10.1016/j.engfailanal.2016.04.027>.
- Yi, Z., Agrawal, A.K., Ettouney, M. and Alampalli, S., (2013), "Blast load effects on highway bridges. I: Modeling and blast load effects", *J. Bridge Eng.*, **19**(4), 04013023. [https://doi.org/10.1061/\(ASCE\)BE.1943-5592.0000547](https://doi.org/10.1061/(ASCE)BE.1943-5592.0000547).
- Zhang, R. and Phillips, B.M. (2016), "Performance and protection of base-isolated structures under blast loading", *J. Eng. Mech.*, **142**(1), 04015063. [https://doi.org/10.1061/\(ASCE\)EM.1943-7889.0000974](https://doi.org/10.1061/(ASCE)EM.1943-7889.0000974).
- Zhang, Y., Zhao, K., Li, Y, Gu, J., Ye, Z. and Ma, J. (2018), "Study on the local damage of SFRC with different fraction under contact blast loading", *Comput. Concrete*, **22**(1), 63-70. <https://doi.org/10.12989/cac.2018.22.1.063>.